Received: 17 September 2021 | Accepted: 19 March 2022

DOI: 10.1002/csc2.20758

Crop Science

ORIGINAL RESEARCH ARTICLE

Crop Breeding & Genetics

Prediction of regrowth and biomass of perennial sorghum using unoccupied aerial systems

Shakirah Nakasagga[1] | **Alper Adak**[1] | **Seth C. Murray**[1] | **William L. Rooney**[1] | **Leo Hoffmann, Jr**[1] | **Scott Wilde**[1] | **Regan Lindsey**[1] | **Pheonah Nabukalu**[2] | **Stan Cox**[2]

[1]Dep. of Soil and Crop Sciences, Texas A&M Univ., 2474 TAMU, College Station, TX 77843, USA

[2]The Land Institute, 2440 E. Water Well Rd., Salina, KS 67401, USA

Correspondence
Seth C. Murray, Dep. of Soil and Crop Sciences, Texas A&M Univ., 2474 TAMU, College Station, TX 77843, USA.
Email: sethmurray@tamu.edu

Assigned to Associate Editor Ramasamy Perumal.

Funding information
Texas A&M AgriLife Research; USDA-NIFA-AFRI, Grant/Award Numbers: 2020-68013-32371, 2021-67013-33915; Eugene Butler Endowed Chair in Biotechnology; Bob Hatch and the Land Institute; USDA-NIFA Hatch funds

Abstract

Perennial grain sorghum [*Sorghum bicolor* (L.) Moench] has potential to produce grain and forage while improving soil health, ecosystem services, and carbon soil sequestration but requires further genetic improvement. Unoccupied aerial systems (UAS, also known as drones and unmanned aerial systems) provide opportunities to quickly evaluate plant traits on a large scale with precision. Unoccupied aerial system flights were used to evaluate biomass yield and rhizome characteristics of 100 diverse sorghum hybrids, most being from an interspecific hybridization program, in the establishment year and first year of regrowth. Twenty-one vegetation indices (VIs) with canopy height measurements (CHMs) were processed from seven UAS flights made temporally during each growing season. Regression of the temporal data (VI and CHM) and phenotypic traits, including rhizome characteristics based on plant stand count (PSC), rhizome-derived shoots (RDS), and fresh and dry biomass yields, showed useful predictions when combining temporal VI with CHM and machine learning. Blue chromatic coordinate index (BCC) best predicted all measured traits. If predictions could be generalized, UAS would reduce field evaluation time for perennial sorghum or breeding perennial grasses in general and allow breeders to evaluate additional genotypes. In this study, we found that optimizing flights to specific dates after planting could minimize resource requirements and costs in prediction of regrowth and biomass yield of perennial sorghum.

1 | INTRODUCTION

Perennial grain crops provide opportunities for environmental conservation by forming plant stands with dense root structures, reducing soil erosion, conserving soil organic matter, reducing inputs, and sequestering carbon (Jessup, 2009; Nabukalu & Cox, 2016). Perennial grain breeding has also registered success in improving grain yield for example kernza, or intermediate wheatgrass (*Thinopyrum intermedium* (Host) Barkworth & DR Dewey subsp. intermedium) (Bajgain et al., 2020; Lanker et al., 2020). Several groups have made interspecific crosses in maize (*Zea mays* L.), wheat (*Triticum aestivum* L.), pearl millet [*Pennisetum glaucum* (L.) R. Br.], rice (*Oryza sativa* L.), and sorghum [*Sorghum*

Abbreviations: BCC, blue chromatic coordinate index; CHM, canopy height measurement; LASSO, least absolute shrinkage and selection operator; MAE, mean absolute error; PSC, plant stand count; RDS, rhizome-derived shoot; RGB, red–green–blue; TBLUP, temporal best linear unbiased prediction; UAS, unoccupied aerial systems; VI, vegetation index.

bicolor (L). Moench] in an attempt to combine rhizome-based perenniality from wild relatives with seed production of domesticated cultivars (Cox et al., 2002; Murray & Jessup, 2013; Scheinost et al., 2001). Rhizomes are horizontal underground storage stems with the capacity to enter a dormant phase under unfavorable weather, typically the cold of winter, followed by regrowth when conditions are conducive (Cox et al., 2002). Dormant season survival is a major challenge for perennial grain and perennial dual-use grain and forage crops.

There is ongoing research in breeding perennial sorghum for grain, forage, and bioenergy. Among the three perennial sorghum species, Johnsongrass [*Sorghum halepense* (L.) Pers] was originally introduced to the United States specifically as a forage species before it became a major weed (McWhorter, 1972). The two other perennial sorghum species [*S. propinquum* (Kunth) Hitch. and almum sorghum (*S.* ×*almum* Parodi)] are less common (De Wet, 1978; Doggett, 1976; Pritchard, 1965). Domesticated sorghum is traditionally grown as an annual crop for grain, grazing, and baling (Saeed et al., 1986). Sorghum/Johnsongrass and Sorghum/*S. propinquum* crosses are reported to have intermediate phenotypes between the parents, that is, taller than either parent, producing numerous aerial tillers with <10% rhizome mass vs. the perennial parent sufficient for overwintering, but not enough to become aggressive weeds (Piper & Kulakow, 1994).

Characterizing rhizomes in perennial sorghum has been done by counting the number of plants per line, plant stand count (PSC), the number of rhizome-derived shoots (RDS), underground rhizome buds, and measuring the distance from the plant crown to the RDS (Paterson et al., 1995; Washburn et al., 2013). Estimating aboveground biomass yield in these materials is a destructive process performed at harvest, which is directly relevant for evaluating forage or bioenergy potential of genotypes. The field activities involved in characterizing rhizomes and estimating biomass, as explained above, are expensive and laborious.

Unoccupied aerial systems (UAS, also known as drones) are now used in some plant breeding programs to measure various phenotypic traits (Bort et al., 2005; Singh et al., 2019). This technology has been shown to increase precision and reduce evaluation time of different plant traits from large fields (Lane & Murray, 2021; Lee et al., 2010). We hypothesize that UAS data could be predictive and useful in rhizome characterization in addition to estimating biomass accumulation nondestructively throughout crop growth. This study attempted to address time and resource constraint challenges in regrowth and biomass evaluations by employing UAS flights temporally throughout plant growth.

Unoccupied aerial systems phenotypic traits, including plant height, leaf area index, biomass and grain yield, among others, have been predicted temporally from vegetation indices (VIs) with canopy height measurements (CHMs) extracted from UAS data (Anderson et al., 2019; Hunt et al., 2005; Marino & Alvino, 2021; Svensgaard et al., 2021). Vegetation indices with CHM can provide important information on the growth, light interception, and organic carbon from both vegetation and the environment (Li et al., 2015). Defined as quantitative measurements indicating the vigor of vegetation, VIs consist of ratios of different spectral bands of canopy reflectance (Campbell, 1987), which are more effective than individual spectral bands (Asrar et al., 1984; Hansen & Schjoerring, 2003; Kross et al., 2015; Rasmussen et al., 2016; Svensgaard et al., 2021). Vegetation absorbs solar radiation from the visible spectrum (400–700 nm); specifically, chlorophyll a and b absorb the blue–violet and red–blue regions to provide energy for photosynthetic activity. Estimates of CHMs are defined as distance above the terrain surface; CHMs have been used to estimate plant height of crops such as sorghum, maize, and wheat (Campbell, 1987; Li et al., 2016; Watanabe et al., 2017; Yue et al., 2017). When measured repeatedly across growth, temporal measurements of VI with CHM can reveal trends throughout the season that arise from interactions between genotypes and the environments (Adak, Conrad et al., 2021; Anderson et al., 2019).

Prediction modeling of agronomic traits improves when temporal measurements of VIs with CHMs are used instead of manual single time-point measurements (Báez-González et al., 2002; GopalaPillai & Tian, 1999). Regression models that can dissect factors involved in phenotypic expression are useful in studying crop traits. Machine-learning methods are important in prediction modeling for decision making in high-throughput phenotyping and genotyping studies when large numbers of factors are involved and without overfitting (Esposito et al., 2020). Ridge, elastic net, and least absolute shrinkage and selection operator (LASSO) models have been widely applied in prediction of quantitative traits and found to have relatively high predictive ability (Arruda et al., 2015; Ogutu et al., 2012). These machine-learning models minimize the problem of multicollinearity, including temporal, within datasets when compared with linear regression (partial least square regression) (Adak, Murray et al., 2021). In addition, ridge regression is reported to minimize error variance

Core Ideas

- Vegetation indices (VIs) can predict plant stand counts for regrowth.
- Blue chromatic coordinate index predicted all assessed traits best.
- Machine learning improved predictive ability.
- Combining VIs with canopy height improved predictive ability for all traits.
- Unoccupied aerial systems can reduce field evaluation time and costs for breeding perennial sorghum.

within very small datasets (Bayo et al., 2021). Given the above advantages, this research evaluated ridge, LASSO, and elastic net regression models in addition to linear regression to predict rhizome characteristics and biomass of perennial sorghum.

The main objective of this study was to investigate the ability of UAS to predict regrowth and assess biomass accumulation for interspecific sorghum hybrids derived from *S. bicolor*/*S. halepense* and *S. bicolor*/*S. propinquum*. We specifically (a) evaluated and compared regression approaches to predict rhizome characteristics and biomass yield and (b) assessed the predictive ability of VIs with CHMs to predict early season regrowth and biomass yield.

2 | MATERIALS AND METHODS

2.1 | Germplasm

The study evaluated 100 sorghum pedigrees (genotypes), primarily comprising perennial derived sorghums, including 80 BC_1F_1 progenies of 'BTx623' × 'Gypsum'. This cross was made using a tetraploid version of BTx623 (Sorghum) hybridized to Gypsum (Johnsongrass). These progenies were selected in Salina, KS, for rhizome characteristics and grain yield using methods described by Nabukalu and Cox (2016). In addition, 13 progenies derived from the cross BTx623 × *S. propinquum* (Washburn et al., 2013), one Johnsongrass line (Gypsum), and six Sorghum (one BTx623 diploid line, one BTx623 tetraploid line, and four grain sorghum hybrids [RTx436, RTx437, NP32_PI535776, and Low-HCN-PRP2B]) (Rooney et al., 2003) were included.

2.2 | Experimental design and establishment

Field experiments were established at the Texas A&M AgriLife Research farm in Burleson County, College Station, TX. These tests were planted in 2019 (seed year) and maintained through 2020 (regrowth year). A randomized complete block design with two replications and single-row plots of 6-m length and 1.5-m width was used. Agronomic practices standard for forage sorghum production were followed (Schnell et al., 2019).

2.3 | Data collection

2.3.1 | Field phenotyping

The evaluation for rhizome characteristics was based on a modified procedure described by Paterson et al. (1995) and Washburn et al. (2013). Briefly, plants per plot were counted (PSC) and three plants were randomly selected from which the RDS per plant were counted.

Plant biomass yield was measured at the end of the growing season in August by harvesting the whole plot using a John Deer 7300 forage harvester equipped with a 130S RCI weigh bucket and sampler. In addition to fresh weight of the plot, a 500-g sample was obtained and weighed. This sample was dried in a forced air oven at 57 ˚C for 5 d. At this point, the sample was reweighed as dry weight. The biomass yields reported herein are on a dry matter basis.

TABLE 1 Dates of unoccupied aerial system flights along with calendar months and days in relation to planting on 2 Apr. 2019 with flights in 2019 seed and 2020 regrowth years

Flight date	Days after planting
30 May 2019	58
4 June 2019	63
11 June 2019	70
19 June 2019	78
9 July 2019	98
12 July 2019	101
22 July 2019	111
14 May 2020	408
19 May 2020	413
5 June 2020	430
11 June 2020	436
20 June 2020	445
6 July 2020	461
12 July 2020	467

2.3.2 | Unoccupied aerial systems

Unoccupied aerial systems data were collected from the sorghum field using a rotary wing-DJI Phantom 4 Pro V2.0 Quadcopter (DJI) with its native red–green–blue (RGB) camera. The UAS was flown 25 m above the ground at 90% forward and side image overlap. In each year, seven flights were used to measure growth (and regrowth) from May through July (Table 1).

2.4 | Data analysis

The manually phenotyped measurements of PSC and RDS (rhizome characteristics) and biomass yield were analyzed to generate the best linear unbiased predictions for each pedigree (genotype). A factorial design with random effects

(row, range, replication, and pedigree) was used in JMP Pro v15 (SAS Institute Inc.) using the following equation:

$$rY_{ijkl} = \mu + \text{row}_i + \text{range}_j + \text{replication}_k + \text{pedigree}_l + \text{error}_{ijkl} \quad (1)$$

where Y_{ijkl} represents individual observations of each of the 100 pedigrees, μ is the grand mean, row_i is effect of the row, range_j is the effect of the range, replication_k is the effect of the replication, pedigree_i is the effect of pedigree, and error_{ijkl} represents the pooled error for all the mentioned factors in Equation 1. Repeatability was calculated as in Equation 2:

$$\text{Repeatability} = \frac{\text{pedigree variance}}{\text{pedigree variance} + \frac{\text{error variance}}{\text{no. of replications}}} \quad (2)$$

For the UAS data, georeferenced orthomosaics and three-dimension point clouds were created from the RGB images using Agisoft Metashape v1.6 (Agisoft LLC, 2020). Orthomosiacs were used to estimate CHMs and biomass accumulation as a function of time during the growing season. Environmental Systems Research Institute (ESRI) shape files were created in R using the UAStools package according to Anderson et al. (2020). The shape file consisted of a polygon for a single-row plot to extract plot information and point clouds for the VIs with CHMs, respectively, from the images for each flight. The FIELDImageR package was used to extract VI from the images (Matias et al., 2020). In conjunction with the shape file, the hue index was used to remove the soil from the images (Escadafal, 1993). Twenty-one VIs were extracted to identify the best predictors for rhizome characteristics and biomass yield (Table 2). Three-dimensional point clouds were used to extract CHMs following Anderson et al. (2019). Extreme points above and below the bare ground were removed from the point clouds using CloudCompare (v2.12 alpha). Software for FUSION/LDV (McGaughey, 2016) and LAStools (Isenburg, 2014) were imported into R to create an extraction pipeline for CHMs for each flight date. The CHM was obtained by subtracting the digital terrain model from the digital surface model (DSM), from which plot-based heights were based as percentile metrics; the 99th percentile is reported.

The UAS data (VI with CHM) from 2019 and 2020 were analyzed separately because each flight date was unique; thus, a combined analysis across years with synchronized dates could not be performed. From these data, the temporal best linear unbiased predictions (TBLUPs) for the VI with CHM for each pedigree were obtained from each flight. Similarly, a random model using a nested design was used in JMP Pro v15 (SAS Institute Inc.) using Equation 3:

$$Y_{ijklm} = \mu + \text{flight}_i + [\text{pedigree}(\text{flight})]_{ik} + [\text{row}(\text{flight})]_{il} + [\text{replication}(\text{flight})]_{im} + \text{error}_{ijklm} \quad (3)$$

where Y_{ijklm} refers to individual observation of each pedigree at ith flight date (days after planting), μ is the grand mean, flight_i is the effect of the ith flight date, $[\text{pedigree(flight)}]_{ij}$ is the effect of the jth pedigree within the ith flight date, $[\text{range(flight)}]_{ik}$ is the effect of the kth range withing the ith flight date, $[\text{row(flight)}]_{il}$ is the effect of the lth row within ith flight date, $[\text{replication (flight)}]_{im}$ is the effect of the mth replication within the ith flight date, and error_{ijkl} represents the pooled error for the mentioned factors in Equation 2.

In total, 154 predictors corresponding to the 22 temporal measures (21 VIs with one CHM) and seven flight dates were used in four regression-based approaches: linear (partial least square regression) and three machine-learning types (LASSO, ridge, elastic net) for each year. It was expected that the machine-learning models would have reduced error variation compared with linear regression because these minimize multicollinearity of predictor variables. LASSO and elastic net minimize model overfitting. In addition, because we were evaluating a segregating population, we expected some missing plots for the pedigrees that would not regenerate; thus, ridge regression was included to minimize error in a reduced dataset. The mentioned regression models were run using the caret package in R.

A cross-validation was performed for each regression model with the dataset split into training and validation sets of 70 and 30%, respectively, with 20 resampling iterations (folds = 20) and three repeated k-fold cross-validations (repeats = 3). Comparisons between the regression models evaluated the coefficient of determination (R^2), lowest root mean square error (RMSE), and lowest mean absolute error (MAE) for each trait. Predictive ability for each regression model in prediction of the assessed traits (PSC, RDS, and fresh and dry biomass yield) was determined using 1,000 bootstrap iterations. The predicted results were then correlated with the actual values in each bootstrap.

A correlation analysis between each time point across VI with CHM for each trait and between TBLUPs across different VIs and time measurements was conducted to identify the best timing for flights and evaluate multicollinearity among temporal data, respectively. In addition, temporal variable importance of the TBLUPs was calculated using the 'varImp' function, ranging from 0 to 100, to demonstrate the importance of VI with CHM in the prediction of rhizome characteristics and biomass yield across the machine-learning techniques (LASSO, elastic net, ridge) for 2019 and 2020. Visualization of the predictions was done using the ggplot2 package in R studio (v1.3.959).

TABLE 2 Red–green–blue-based vegetation indices (VIs) with their respective band ratios used in this study

VI	Common name	Equation	Reference
R	Red	R	Bending et al., 2015
G	Green	G	Bending et al., 2015
B	Blue	B	Woebbecke et al., 1995
NGRDI	Normalized green–red difference index	$(G-R)/(G+R)$	Hunt et al., 2005
RGBVI	Red–green–blue vegetation index	$(G^2-BR)/(G^2+BR)$	Bending et al., 2015
MGVRI	Modified green–red vegetation index	$(G^2-R^2)/(G^2+R^2)$	Bending et al., 2015
VARI	Visible atmospherically resistant index	$(G-R)/(G+R-B)$	Gitelson et al., 2002
BGI	Blue–green pigment index	B/G	Zarco-Tejada et al., 2005
BI	Brightness index	$\sqrt{(R^2+G^2+B^2)/3}$	Richardson & Wiegand, 1977
EXG	Excessive green index	$2G-B-R$	Woebbecke et al., 1995
EXGR	Excess green minus excess red index	EXG2 − EXR	Meyer & Neto, 2008
GLI	Green leaf index	$(2G-R-B)/(2G+R+B)$	Louhaichi et al., 2001
NGBDI	Normalized green–blue difference index	$(G-B)/(G+B)$	Du & Noguchi, 2017
VEG	Vegetative index	$G/(R^{0.667}B^{0.334})$	De Swaef et al., 2021
BCC	Blue chromatic coordinate index	$B/(R+G+B)$	De Swaef et al., 2021
RCC	Red chromatic coordinate index	$R/(R+G+B)$	De Swaef et al., 2021
EXR	Excess red index	$(1.4R-G)/(R+G+B)$	De Swaef et al., 2021
EXG2	Excess green index v2 index	$(2G-B-R)/(R+G+B)$	De Swaef et al., 2021
BRVI	Blue–red vegetation index	$(B-R)/(B+R)$	De Swaef et al., 2021
G/R	Green–red ratio index	G/R	De Swaef et al., 2021
G-R	Green–red difference index	$G-R$	De Swaef et al., 2021

3 | RESULTS

3.1 | Field phenotyping outputs

In both 2019 and 2020, pedigrees were not significantly different ($p = .076$ and .72, respectively) for RDS. In 2020, RDS were reduced compared with 2019. Pedigrees were significantly different for PSC in both years ($p < .001$ and .012, respectively). Biomass yields (fresh and dry) varied with pedigrees in 2019 ($p < .001$) but not in 2020. In general, means for all traits were lower in 2020 than in 2019, resulting in overall fewer significant differences between pedigrees (Table 3).

In 2019, the contribution of pedigree was the largest to variation for PSC, fresh and dry matter yields, with a high degree of repeatability. Rhizome-derived shoots had a very low repeatability and was explained by the high percentage error variation. In 2020, a moderate-to-high percentage error variation was recorded across all phenotypic traits, reducing their repeatability substantially. Repeatability for RDS was practically zero (Table 4).

3.2 | Evaluation of vegetation indices VI with CHM

Among UAV extracted data, pedigrees were significantly different for all 21 VIs across the seven flights ($p < .001$) in 2019, but pedigrees had no effect on any VI in 2020. For

TABLE 3 Summary statistics for raw field phenotypic data for 2019 and 2020

	Year							
	2019				2020			
	RDS	PSC	Fresh matter yield	Dry matter yield	RDS	PSC	Fresh matter yield	Dry matter yield
	No.		kg ha^{-1}		No.		kg ha^{-1}	
Min.	0	1	1,171	510	0	0	195	0
Max.	9	33	67,770	31,446	6	14	33,397	15,931
Mean	3	15	26,612	11,710	1	8	12,725	6,140
SD	2	6	15,207	6,760	1	3	6,388	3,100

Note. RDS, rhizome derived shoots; PSC, plant stand count.

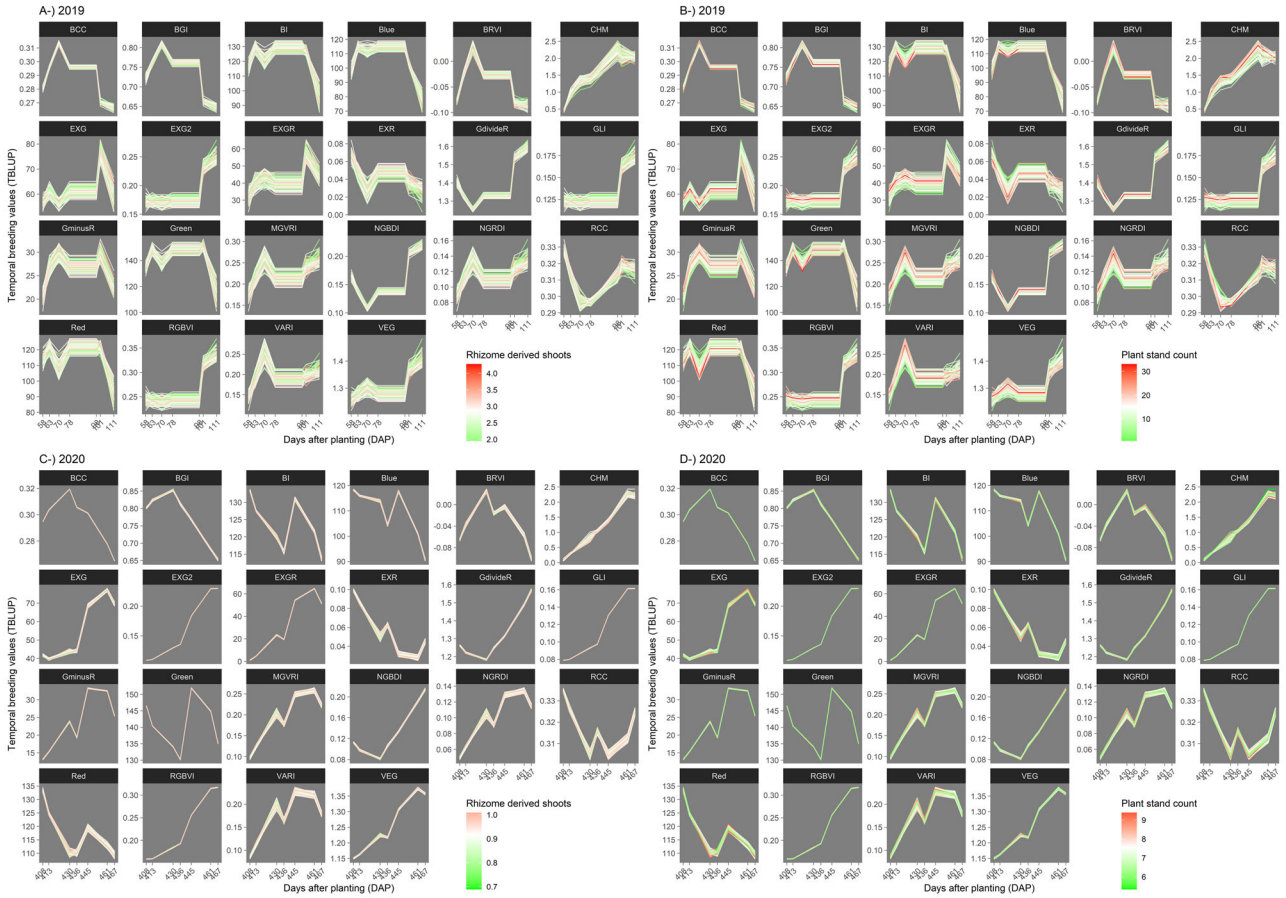

FIGURE 1 Temporal best linear unbiased predictions (TBLUPs) of the assessed vegetation indices (VIs) with canopy height measurements (CHM)-upper right corner of the pedigrees for 2019 (left) and 2020 (right). The *y* axes shows the range of TBLUPs while *x* axes shows the flight dates as days after planting (DAP) with the rhizome derived shoots (above) and plant stand count (left) BLUP values of the pedigrees

CHM, pedigrees were significantly different in both 2019 and 2020 ($p = .0002$ and $p = .019$, respectively). The flight dates between years (the day the UAS was flown) were also significantly different for CHM ($p < .001$). In 2020, TBLUPs for VIs were compressed likely because of the lower means and winter mortality.

The VIs blue–green pigment index, blue chromatic coordinate index (BCC), blue–red vegetation index, brightness index, Blue, Green, Red, excessive green index, excess green minus excess red index, green–red difference index, normalized green–red difference index, red–green–blue vegetation index, , vegetative index (Table 2) typically followed a concave pattern (curving inwards) of overgrowth in both years where sparse or senesced plants had the highest values and healthy plants the lowest. The VIs excess green index v2 index, green–red ratio index, green leaf index, , normalized

TABLE 4 Percentage variation and repeatability for the field phenotypic data for 2019 and 2020

	n	Year							
		2019				2020			
		RDS	PSC	Fresh matter yield	Dry matter yield	RDS	PSC	Fresh matter yield	Dry matter yield
		%							
Pedigree	100	15.099	59.424	71.837	73.371	0	22.135	1.018	8.47
Row	13	0.925	13.78	8.257	8.428	6.519	2.851	16.647	11.176
Range	16	14.726	10.548	5.042	3.489	17.783	23.563	14.151	16.674
Replication	2	4.481	3.087	0.983	0.428	0	0	0	0
Error	–	64.769	13.16	13.88	14.283	75.698	51.451	68.184	63.681
Repeatability	–	0.091	0.953	0.912	0.834	0	0.462	0.029	0.21

Note. *n*, number of levels of observations; RDS, rhizome derived shoots; PSC, plant stand count.

green–blue difference index, normalized green–red difference index, red chromatic coordinate index, red–green–blue vegetation index, , vegetative index, and, green–red ratio index, normalized green–blue difference index, red chromatic coordinate index had a convex pattern (curving outwards), where sparse or senesced plants had the lowest values and healthy plants the highest. Vegetation index BCC showed the clearest pattern across the growing season for the RDS, PSC, and fresh and dry matter yields compared with other indices in both years. The CHM displayed a sigmoid pattern in both years (Figures 1 and 2).

Temporal correlations of each time point across VIs with CHMs for each trait (Figure 3) showed wide variation seen from the different trends displayed in 2019 and 2020. Temporal correlations for RDS ranged from −0.25 to 0.1 across all VIs with CHMs, most registering zero across the flight dates in both years. The PSC and fresh and dry matter yields displayed a wider range from −0.5 to 0.5, fluctuating across flight dates for VIs with CHMs in 2019. This range halved to −0.25 to 0.25 in the regrowth year (2020), reducing predictability of PSC and fresh and dry matter yields from the temporal measurements. Correlation analysis between TBLUPs across different VI and time measurements showed values changing between −1 to 1 (Figure 4). Temporal correlations in 2019 fluctuated less than in 2020. Overall, correlations were low to moderate between VIs, demonstrating different VIs were not redundant and provided different information. Similarly, for some VIs, moderate correlations were observed temporally within a single trait. When the same VIs are less correlated at different time points, this means more unique information is provided by additional time points to use in prediction; thus, temporal variable importance was emphasized.

For the temporal variable importance, some VIs predicted RDS, PSC, and fresh and dry matter yields across all flight dates throughout growth, whereas others predicted these phenotypes better at specific flight dates and stages. The VI BCC best predicted RDS at 101 d (Year 1) and 430 d (regrowth, Year 2) in 2019 and 2020, respectively, using ridge regression (Figure 5). The PSC was consistently best predicted by BCC throughout (63, 78, and 98 d) with ridge regression and by the RCC at 101 d for the elastic net and LASSO regression models in 2019. In 2020, the BCC moderately predicted PSC at 430 and 461 d; at 467 d, the red–green–blue vegetation index for the LASSO and EXG2 and green leaf index for the elastic net gave consistent and best predictions. This was at maturity when the plants were fully established. For both fresh and dry matter yields, BCC consistently best predicted biomass in 2019, specifically at 63 and 70 d across all regression models. Throughout days 63, 70, 78, and 98, BCC consistently predicted dry and fresh matter yield well using elastic net regression. In 2020, BCC consistently predicted both dry and fresh matter yield well using ridge regression at 430 d. Vegetation indices BCC and green leaf index predicted dry and fresh matter yield well at 430 and 467 d, respectively, for the elastic net regression.

3.3 | Regression model evaluation

Linear regression of VIs with CHMs in prediction of the RDS, PSC, and fresh and dry matter yields had the highest RMSE and MAE (Table 5) in both years. Elastic net and LASSO regression were also ineffective in modeling RDS in 2019 and in both years, respectively.

3.4 | Predictive ability

The predictive ability of VIs combined with CHMs was greater for the machine-learning models than linear regression (Figure 6). Slight differences were observed between machine-learning models (elastic net, ridge, and LASSO) with respect to predictive ability for the VIs with CHMs. All machine-learning methods had predictive abilities >70%,

TABLE 5 Model comparison using all the vegetation indices and canopy height measurements. The coefficient of determination (R^2), root mean square error (RMSE), and mean absolute error (MAE) of the rhizome derived shoots, plant stand count, fresh and dry matter yields for 2019 and 2020

		Rhizome-derived shoots			Plant stand count			Fresh matter yield			Dry matter yield		
Statistic	**Model**	**Mean**	**Min**	**Max**	**Mean**	**Min**	**Max**	**Mean**	**Min**	**Max**	**Mean**	**Min**	**Max**
2019													
R^2	Linear	.23	.0023	.70	.23	.0016	.90	.16	.000011	.63	.17	.000014	.65
	Elastic net	.20	.000071	.72	.54	.063	.93	.62	.17	.84	.61	.095	.92
	Ridge	.18	.000098	.60	.49	.042	.89	.64	.0000011	.97	.63	.20	.94
	LASSO	NA	NA	NA	.52	.017	.87	.59	.038	.87	.52	.099	.98
MAE	Linear	5.67	1.14	22.82	53.44	4.18	295.21	141.366.10	19,047.90	748,461.17	110,803.34	10,268.06	1,435,778.37
	Elastic net	0.34	0.26	0.53	2.87	1.49	4.98	7,249.19	3,398.30	11,067.67	3,166.91	1,314.43	6,634.78
	Ridge	0.34	0.17	0.58	3.11	1.32	5.66	7,745.43	4,127.42	11,083.37	3,150.56	1,750.31	4,679.96
	LASSO	0.35	0.24	0.55	2.97	1.26	4.24	7,884.87	4,229.20	12,473.58	3,429.38	1,632.60	4,955.36
RMSE	Linear	6.93	1.45	27.68	66.18	4.97	350.22	173,560.61	24,956.57	943,385.20	142,101.30	12,820.89	1,954,317.04
	Elastic net	0.43	0.33	0.69	3.53	2.04	6.07	9,332.07	4,690.42	12,933.88	3,824.51	1,884.40	7,217.04
	Ridge	0.42	0.22	0.70	3.87	1.45	6.99	9,645.06	4,974.09	14,378.78	3,842.27	2,090.30	5,499.87
	LASSO	0.44	0.30	0.72	3.72	1.58	5.75	9,815.56	4,912.99	14,698.90	4,152.15	1,766.67	5,993.57
2020													
R^2	Linear	.14	0	.48	.18	.000029	.75	.17	.003	.79	.17	.00016	.83
	Elastic net	NA	NA	NA	.23	.00047	.68	.38	.019	.80	.28	.0000082	.87
	Ridge	.16	0	.72	.19	.000011	.93	.31	.0085	.86	.19	.00013	.64
	LASSO	NA	NA	NA	.15	.00052	.64	.37	.0016	.89	.28	.00066	.90
MAE	Linear	0.83	0.14	6.10	13.54	2.54	84.14	4,673.5	317.69	78,531.90	5,125.77	1,093.38	26,330.01
	Elastic net	0.042	0.025	0.07	0.78	0.51	1.03	85.37	34.02	137.45	379.27	228.95	618.85
	Ridge	0.044	0.027	0.068	0.79	0.37	1.07	80.30	33.10	122.73	350.38	197	517.06
	LASSO	0.042	0.024	0.079	0.79	0.50	1.01	89.24	43.86	147.91	412.57	195.29	840.24
RMSE	Linear	1.07	0.15	8.23	16.64	3.45	107.38	6,025.85	366.62	97,076.72	6,055.78	1,297.98	29,127.72
	Elastic net	0.055	0.032	0.10	0.95	0.66	1.22	106.86	41.69	164.67	467.93	235.28	747.23
	Ridge	0.056	0.034	0.098	0.96	0.46	1.31	100.74	47.76	160.95	425.40	244.68	672.83
	LASSO	0.055	0.027	0.11	0.96	0.71	1.25	108.24	52.57	176.91	512.27	232.07	1,001.93

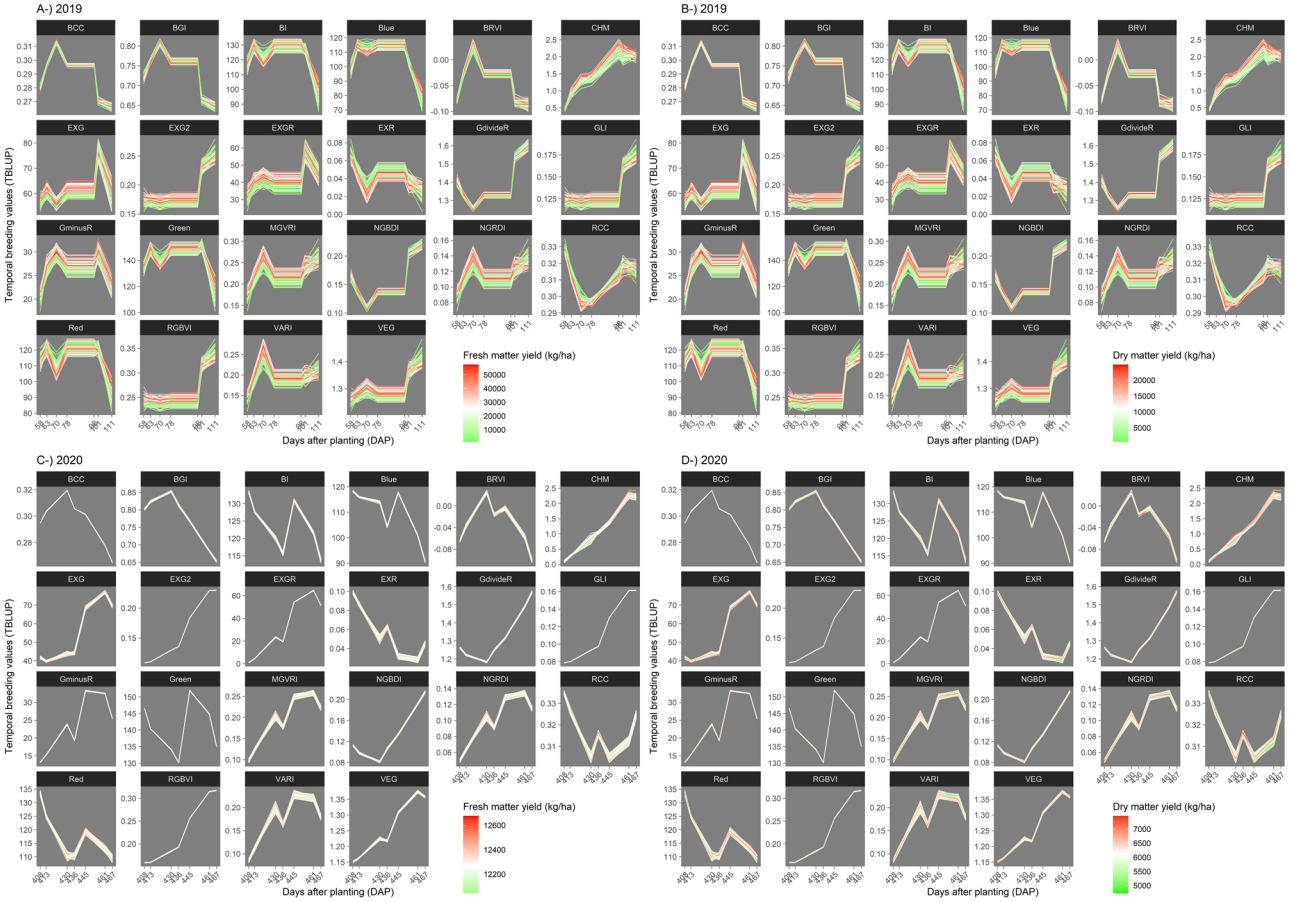

FIGURE 2 Temporal best linear unbiased predictions (TBLUPs) of the assessed vegetation indices (VIs) with canopy height measurements (CHM)-upper right corner of the pedigrees for 2019 (left) and 2020 (right). The *y* axes shows the range of TBLUPs while *x* axes shows the flight dates as days after planting (DAP) with the fresh (above) and dry (below) matter yield BLUP values of the pedigrees

whereas the linear model had <10% predictive ability for the PSC and dry and fresh matter yields in 2019 (Figure 6). The predictive abilities decreased in 2020 across all models for the PSC and dry and fresh matter yield. A similar trend was seen for the RDS, which also had a much lower predictive ability than the rest of the traits in the previous year (2019) and was essentially not predictable in 2020.

4 | DISCUSSION

A general trend in reduction of RDS, PSC and fresh and dry matter yields was observed in 2020 across all pedigrees. This reduction was likely a result of winterkill; however, many factors can contribute to plant death and these appeared to be uneven, substantially lowering even the repeatability between replicates. The average survivability from the establishment year to the second year was 53%, likely because many of these progenies were still segregating for rhizome and perennial characteristics including within plots. This could be a limitation to predicting regrowth from UAS data; however, with additional selection and less segregation, UAS could still be very useful in providing objective measures. Yield reductions in regrowth compared with the main crop are common and have been reported in many short-lived herbaceous perennials (Singh & Singh, 2002; Singh et al., 2005; Sundara, 1997).

The different temporal measurements (VIs with CHMs) displayed varied patterns across growth (Figures 1 and 2). The compression of RDS, PSC and fresh and dry matter yields in 2020 TBLUPs likely were due to the lower plot means. Vegetation indices typically display a concave pattern (inward curve) across a full growth season and are characterized with low values at early growth stages, because of a very sparse canopy, and in the late stage because of leaf senescence. The VI increases as the plant develops and accumulates vegetative biomass and then decreases during postanthesis to physiological maturity of seed (Stanton et al., 2017; Vina et al., 2004). The CHM is characterized by a sigmoidal pattern, with initial increment at a decreasing rate followed by a rapid increase to a critical point then to a constant or eventual decline (Adak, Murray et al., 2021; Anderson et al., 2019; Chang et al., 2017). Because we obtained atypical patterns (convex) for some VIs, additional flights would likely improve the statistical power in predicting the temporal UAS breeding values of VIs with

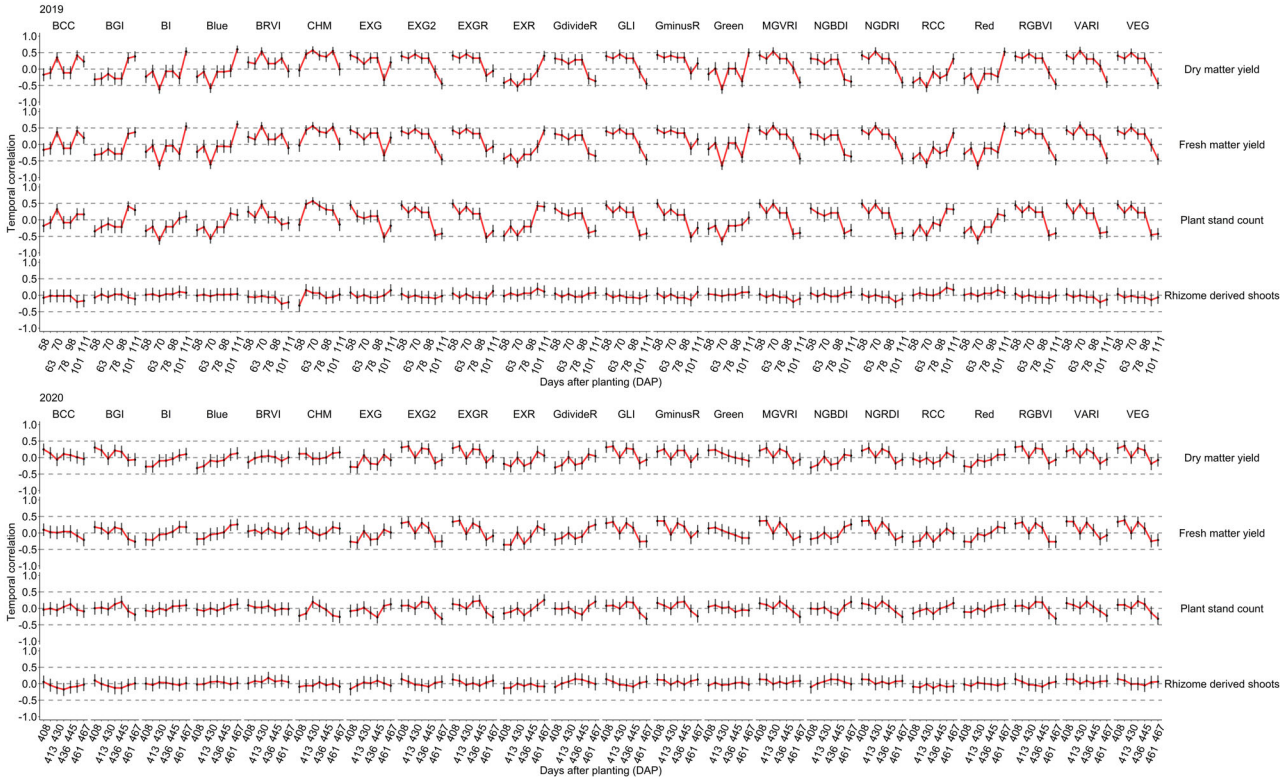

FIGURE 3 Temporal correlation of each time point for 2019 (above) and 2020 (below). The *y* axes shows the range of flight means unique to each trait, whereas the *x* axes shows the flight dates

CHMs, but this would also increase resources required. To address this constraint, optimizing flights to specific dates after planting would minimize resource requirements and costs in prediction of the traits of interest. Toward this, informative correlations for each trait between each VI with CHM time point would help in optimizing flights to specific dates after planting. However, many correlations obtained in this study were too low and inconsistent (Figure 3) to identify suitable time points for flights in assessment of RDS, PSC and fresh and dry matter yields. Correlation analysis between TBLUPs across different VIs and time measurements was highly inconsistent (Figure 4), meaning multicollinearity was not a problem and the entirety of temporal data collected can be used for prediction in subsequent studies.

Temporal variable importance was useful in identifying the most important time points and VIs across the growth season for flights and evaluation of phenotypic traits. In some cases, a VI predicted RDS, PSC and fresh and dry matter yields across a series of dates, whereas others predicted RDS, PSC and fresh and dry matter yields at specific dates and stages across the growth season (Figure 5). For example, VI BCC best predicted RDS at 101 d (Year 1) and 430 d (Year 2), which is consistent with previously reported timing for rhizome development (Horowitz, 1972) where more RDS are expected at flowering and later in the season. In 2020, most of the regrowth regenerated from the rhizomes, so RDS were expected earlier in the season; however, RDS ended up being inconsistent. Overall, the most valuable flights were in the early-to-middle season for VI, whereas for CHM, no particular flight dates could be identified as the best for predicting RDS, PSC and fresh and dry matter yields. Further studies are needed to determine if such times exist.

Vegetation index BCC was identified as the best predictor of all traits in both years. The BCC measures blue light relative to red and green light (De Swaef et al., 2021). Woebbecke et al. (1995) reported that chromatic coordinates provided more variation than individual RGB coordinates (Woebbecke et al., 1995), and for this study, BCC was the most predictive. If BCC predictions can be generalized, it could reduce time required to manually phenotype these traits, which would speed up the selection process.

Plant stand counts for the regrowth predicted rhizome characteristics much more efficiently than RDS across VIs and CHMs. Plant stand counts also are easier to evaluate than examining individual plants for RDS, which had very low to negligible repeatability. Plant stand counts in the spring are an indirect measure of the previous RDS measurement because 90% of perennial growth in sorghum regenerates from rhizomes (Nabukalu & Cox, 2016). Further, plants originating from the crown, in addition to rhizomes, would be included; thus, PSC is likely the most robust means for measuring perennial characteristics. A limitation is that because

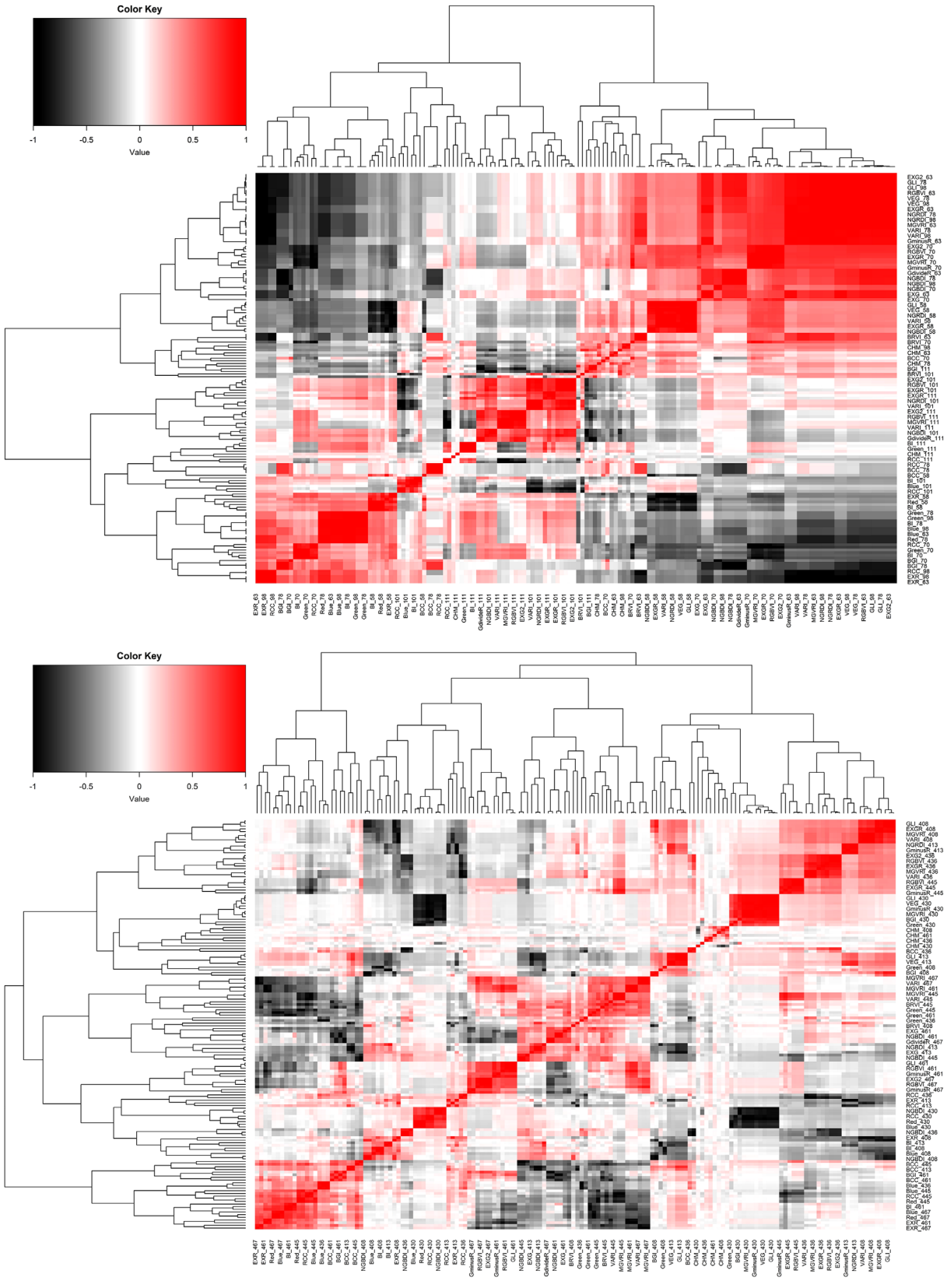

FIGURE 4 Pearson correlation coefficients between Temporal best linear unbiased predictions across different vegetation indices and time measurements for (a) 2019 and (b) 2020

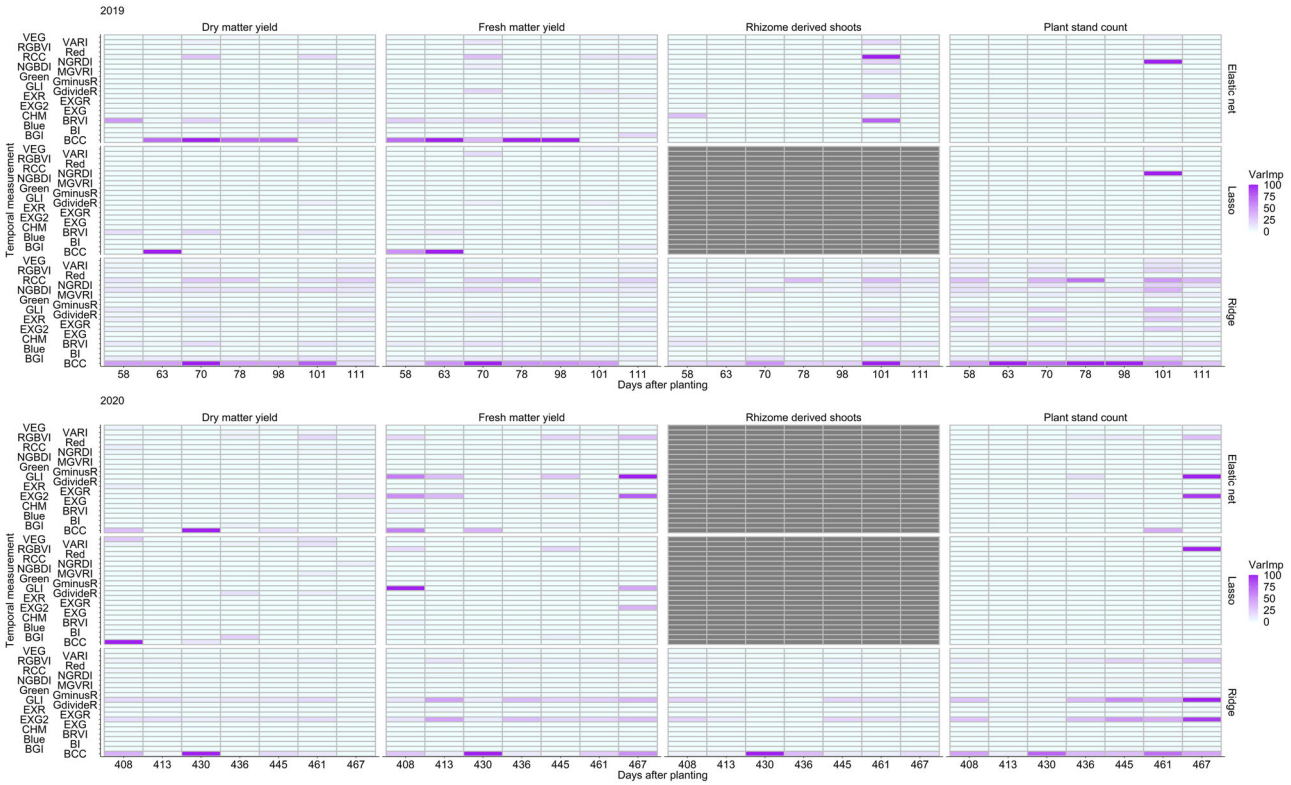

FIGURE 5 Heatmap of temporal variable importance of the predictor traits across seven flight dates in 2019 (above) and 2020 (below) for elastic net, ridge, and LASSO regression models. The *y* axes are identical and represent predictor traits for each regression model, vegetation indices with canopy height measurements. The *x* axes are identical and are flight dates represented as days after planting. Model failed to converge for the greyed out boxes

individual plant assessments are not conducted, desirable plants may be missed in plots still segregating. If UAS methods can be applied to single plants rather than at the plot level, this would improve selection ability, especially for highly genetically segregating plots as measured here. For biomass yield evaluation as well, PSC could be used to select pedigrees that accumulated biomass earlier in the season. This would be especially useful in the early phases of evaluation when genotype numbers are large.

In a breeding program, it is essential to have models that minimize error and correctly rank pedigrees (Adak, Murray et al., 2021). Machine-learning methods minimized error better and had a higher predictive ability than the linear model (Figure 6). Specifically, the ridge regression had the lowest error and showed consistency at modeling all traits in this study (Table 5). Elastic net and LASSO regression were also ineffective in modeling RDS in 2019 and in both years, respectively, possibly because the models failed to converge because of individual year differences. Ideally, years could be combined in training, and a subset of these samples would be tested to predict rhizome characteristics and biomass with improved predictive ability. However, differences in flight dates across environments make combining complicated and, to date, remains a barrier in analysis. Furthermore, because of biological differences in growth rates within and between environments, plants may be at different physiological stages. Determining methods to appropriately deal with these issues would be a major statistical innovation in phenomics-assisted breeding.

In conclusion, combined VIs with CHMs and machine-learning outperformed linear regression. Blue chromatic coordinate index best predicted all measured traits. Optimizing flights to specific dates after planting would minimize resource requirements and costs in prediction of regrowth and biomass yield of perennial sorghum.

ACKNOWLEDGMENTS

The authors acknowledge the Texas A&M University farm crew, sorghum breeding program, and student workers for their assistance in agronomic management and sample processing. Funding for this work was provided by The Land Institute of Salina, KS, through the generous donation of Mr. Bob Hatch, S. Murray's USDA–NIFA Hatch Project and the Eugene Butler Chair.

AUTHOR CONTRIBUTIONS

Shakirah Nakasagga: Conceptualization; Formal analysis; Writing – original draft; Writing – review & editing. Alper

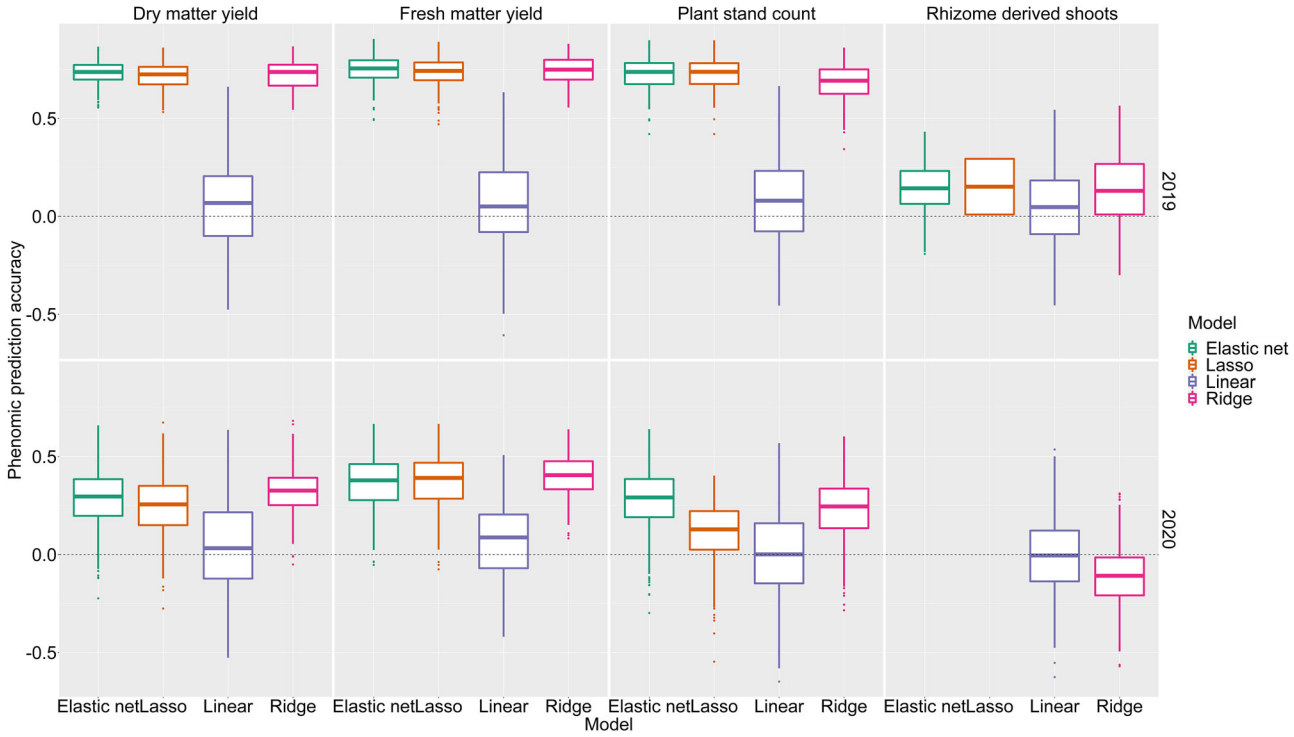

FIGURE 6 Predictive ability of each regression model for dry and fresh matter yields, rhizome derived shoots, and plant stand count using vegetation indices with canopy height model for 2019 and 2020. The *y* axes represent correlation coefficients between the predicted and actual values of the assessed traits. The *x* axes separate the regression models

Adak: Formal analysis; Methodology; Visualization; Writing – review & editing. Seth C. Murray: Conceptualization; Funding acquisition; Project administration; Supervision; Writing – review & editing. William L. Rooney: Methodology; Writing – review & editing. Leo Hoffmann: Data curation; Writing – review & editing. Scott Wilde: Data curation; Writing – review & editing. Regan Lindsey: Data curation. Pheonah Nabukalu: Writing – review & editing. Stan Cox: Funding acquisition; Writing – review & editing.

CONFLICT OF INTEREST

The authors declare no conflict of interest.

ORCID

Shakirah Nakasagga https://orcid.org/0000-0003-3278-1887
Alper Adak https://orcid.org/0000-0002-2737-8041
William L. Rooney https://orcid.org/0000-0001-7953-1856

REFERENCES

Adak, A., Conrad, C., Chen, Y., Wilde, S. C., Murray, S. C., Anderson, S., & Subramanian, N. K. (2021). Validation of functional polymorphisms affecting maize plant height by unoccupied aerial systems (UAS) discovers novel temporal phenotypes. *G3 Genes|Genomes|Genetics*, *11*, jkab075. https://doi.org/10.1093/g3journal/jkab075

Adak, A., Murray, S. C., Božinović, S., Lindsey, R., Nakasagga, S., Chatterjee, S., Anderson, S. L., & Wilde, S. (2021). Temporal vegetation indices and plant height from remotely sensed imagery can predict grain yield and flowering time breeding value in maize via machine learning regression. *Remote Sensing*, *13*, 2141. https://doi.org/10.3390/rs13112141

AgiSoft (2020). *PhotoScan Professional* (v1.6). http://www.agisoft.com/downloads/installer/

Anderson, S. L., Murray, S. C., Chen, Y., Malambo, L., Chang, A., Popescu, S., & Jung, J. (2020). Unoccupied aerial system enabled functional modeling of maize height reveals dynamic expression of loci. *Plant Direct*, *4*, e00223. https://doi.org/10.1002/pld3.223

Anderson, S. L., Murray, S. C., Malambo, L., Ratcliff, C., Popescu, S., Cope, D., Chang, A., Jung, J., & Thomasson, J. A. (2019). Prediction of maize grain yield before maturity using improved temporal height estimates of unmanned aerial systems. *The Plant Phenome Journal*, *2*, 1–15. https://doi.org/10.2135/tppj2019.02.0004

Arruda, M. P., Brown, P. J., Lipka, A. E., Krill, A. M., Thurber, C., & Kolb, F. L. (2015). Genomic selection for predicting Fusarium head blight resistance in a wheat breeding program. *The Plant Genome*, *8*, plantgenome2015.01.0003. https://doi.org/10.3835/plantgenome2015.01.0003

Asrar, G., Fuchs, M., Kanemasu, E. T., & Hatfield, J. L. (1984). Estimating absorbed photosynthetic radiation and leaf area index from spectral reflectance in wheat. *Agronomy Journal*, *76*, 300–306. https://doi.org/10.2134/agronj1984.00021962007600020029x

Báez-González, A. D., Chen, P. Y., Tiscareño-López, M., & Srinivasan, R. (2002). Using satellite and field data with crop growth modeling to monitor and estimate corn yield in Mexico. *Crop Science*, *42*, 1943–1949. https://doi.org/10.2135/cropsci2002.1943

Bajgain, P., Zhang, X., Jungers, J. M., DeHaan, L. R., Heim, B., Sheaffer, C. C., & Anderson, J. A. (2020). 'MN-Clearwater', the first food-grade intermediate wheatgrass (Kernza perennial grain) cultivar. *Journal of Plant Registrations*, *14*, 288–297. https://doi.org/10.1002/plr2.20042

Bayo, A. K., Rafiu, A. B., Funmilayo, A. T., & Oluyemi, O. I. (2021). Investigating the impact of multicollinearity on linear regression estimates. *Malaysian Journal of Computing*, *6*, 698–714.

Bending, J., Yu, K., Aasen, H., Bolten, A., Bennertz, S., Broscheit, J., & Bareth, G. (2015). Combining UAS-based plant height from crop surface models, visible, and near infrared vegetation indices for biomass monitoring in barley. *International Journal of Applied Earth Observation and Geoinformation*, *39*, 79–87. https://doi.org/10.1016/j.jag.2015.02.012

Bort, J., Casadesus, J., Nachit, M. M., & Araus, J. L. (2005). Factors affecting the grain yield predicting attributes of spectral reflectance indices in durum wheat: Growing conditions, genotype variability and date of measurement. *International Journal of remote sensing*, *26*(11), 2337–2358. https://doi.org/10.1080/01431160512331337808

Campbell, J. B. (1987). *Introduction to remote sensing*. Guilford Press.

Chang, A., Jung, J., Maeda, M. M., & Landivar, J. (2017). Crop height monitoring with digital imagery from unmanned aerial system (UAS). *Computers and Electronics in Agriculture*, *141*, 232–237. https://doi.org/10.1016/j.compag.2017.07.008

Cox, T. S., Bender, M., Picone, C., Tassel, D. L., Holland, J. B., & Brummer, E. C. (2002). Breeding perennial grain crops. *Critical Reviews in Plant Sciences*, *21*, 59–91. https://doi.org/10.1080/0735-260291044188

De Swaef, T., Maes, W. H., Aper, J., Baert, J., Cougnon, M., Reheul, D., Steppe, K., Roldán-Ruiz, I., & Lootens, P. (2021). Applying RGB- and thermal-based vegetation indices from UAVs for high-throughput field phenotyping of drought tolerance in forage grasses. *Remote Sensing*, *13*, 147. https://doi.org/10.3390/rs13010147

De Wet, J. M. J. (1978). Special paper: Systematics and evolution of sorghum sect. Sorghum (Gramineae). *American Journal of Botany*, *65*, 477–484. https://doi.org/10.1002/j.1537-2197.1978.tb06096.x

Doggett, H. (1976). Sorghum: *Sorghum bicolor* (Gramineae-Andropogoneae). Evolution of crop plants. In N. W. Simmonds (Ed.), *Evolution of crop plants* (pp. 112–117). Longman.

Du, M., & Noguchi, N. (2017). Monitoring of wheat growth status and mapping of wheat yield's within-field spatial variations using color images acquired from UAV-camera system. *Remote sensing*, *9*, 289. https://doi.org/10.3390/rs9030289

Escadafal, R. (1993). Remote sensing of soil color: Principles and applications. *Remote Sensing Reviews*, *7*, 261–279. https://doi.org/10.1080/02757259309532181

Esposito, S., Carputo, D., Cardi, T., & Tripodi, P. (2020). Applications and trends of machine learning in genomics and phenomics for next-generation breeding. *Plants*, *9*, 34. https://doi.org/10.3390/plants9010034

Gitelson, A. A., Kaufman, Y. J., Stark, R., & Rundquist, D. (2002). Novel algorithms for remote estimation of vegetation fraction. *Remote sensing of Environment*, *80*(1), 76–87. https://doi.org/10.1016/S0034-4257(01)00289-9

GopalaPillai, S., & Tian, L. (1999). In-field variability detection and spatial yield modeling for corn using digital aerial imaging. *Transactions of the American Society of Agricultural and Biological Engineers*, *42*, 1911–1920. https://doi.org/10.13031/2013.13356

Hansen, P. M., & Schjoerring, J. K. (2003). Reflectance measurement of canopy biomass and nitrogen status in wheat crops using normalized difference vegetation indices and partial least squares regression. *Remote Sensing of Environment*, *86*, 542–553. https://doi.org/10.1016/S0034-4257(03)00131-7

Horowitz, M. (1972). Early development of Johnsongrass. *Weed Science*, *20*, 271–273.

Hunt, R. E., Cavigelli, M., Daughtry, C. S. T., & McMurtry, J. (2005). Evaluation of digital photography from model aircraft for remote sensing of crop biomass and nitrogen status. *Precision Agriculture*, *6*, 359–378. https://doi.org/10.1007/s11119-005-2324-5

Isenburg, M. (2014). *Rapidlasso. LAStools: Efficient LiDAR processing software*. v170628. Rapidlasso GmbH. https://rapidlasso.com/LAStools/

Jessup, R. W. (2009). Development and status of dedicated energy crops in the United States. *The Society for In Vitro Biology*, *45*, 282–290.

Kross, A., McNairn, H., Lapen, D., Sunohara, M., & Champagne, C. (2015). Assessment of RapidEye vegetation indices for estimation of leaf area index and biomass in corn and soybean crops. *International Journal of Applied Earth Observation and Geoinformation*, *34*, 235–248. https://doi.org/10.1016/j.jag.2014.08.002

Lane, H. M., & Murray, S. C. (2021). High Throughput can produce better decisions than high accuracy when phenotyping plant populations. *Crop Science*, *61*, 3301–3313. https://doi.org/10.1002/csc2.20514

Lanker, M., Bell, M., & Picasso, V. D. (2020). Farmer perspectives and experiences introducing the novel perennial grain Kernza intermediate wheatgrass in the US Midwest. *Renewable Agriculture and Food Systems*, *35*, 653–662. https://doi.org/10.1017/S1742170519000310

Lee, W. S., Alchanatis, V., Yang, C., Hirafuji, M., Moshou, D., & Li, C. (2010). Sensing technologies for precision specialty crop production. *Computers and Electronics in Agriculture*, *74*, 2–33. https://doi.org/10.1016/j.compag.2010.08.005

Li, W., Niu, Z., Chen, H., Li, D., Wu, M., & Zhao, W. (2016). Remote estimation of canopy height and aboveground biomass of maize using high-resolution stereo images from a low-cost unmanned aerial vehicle system. *Ecological Indicators*, *67*, 637–648. https://doi.org/10.1016/j.ecolind.2016.03.036

Li, W., Niu, Z., Huang, N., Wang, C., Gao, S., & Wu, C. (2015). Airborne LiDAR technique for estimating biomass components of maize: A case study in Zhangye City, Northwest China. *Ecological Indicators*, *57*, 486–496. https://doi.org/10.1016/j.ecolind.2015.04.016

Louhaichi, M., Borman, M. M., & Johnson, D. E. (2001). Spatially located platform and aerial photography for documentation of grazing impacts on wheat. *Geocarto International*, *16*, 65–70. https://doi.org/10.1080/10106040108542184

Marino, S., & Alvino, A. (2021). Vegetation indices data clustering for dynamic monitoring and classification of wheat yield crop traits. *Remote Sensing*, *13*, 541. https://doi.org/10.3390/rs13040541

Matias, F. I., Caraza-Harter, M. V., & Endelman, J. B. (2020). FIELDImageR: An R package to analyze orthomosaic images from agricultural field trials. *The Plant Phenome Journal*, *3*, e20005. https://doi.org/10.1002/ppj2.20005

McGaughey, R. J. (2016). *FUSION/LDV: Software for LIDAR data analysis and visualization. v3.50*. USDA Forest Service–Pacific Northwest Research Station.

McWhorter, C. G. (1972). Factors affecting Johnsongrass rhizome production and germination. *Weed Science Society of America*, *20*, 41–45. https://doi.org/10.1017/S0043174500034901

Meyer, G. E., & Neto, J. C. (2008). Verification of color vegetation indices for automated crop imaging applications. *Computers and Electronics in Agriculture*, *63*, 282–293. https://doi.org/10.1016/j.compag.2008.03.009

Murray, S. C., & Jessup, R. W. (2013). Breeding and genetics of perennial maize: Progress, opportunities and challenges. In *Perennial crops for food security, Proceedings of the FAO Expert Workshop, 28–30 August 2013, Rome, Italy* (pp. 103–111). Food and Agricultural Organization.

Nabukalu, P., & Cox, T. S. (2016). Response to selection in the initial stages of a perennial sorghum breeding program. *Euphytica*, *209*, 103–111. https://doi.org/10.1007/s10681-016-1639-9

Ogutu, J. O., Schulz-Streeck, T., & Piepho, H. P. (2012). Genomic selection using regularized linear regression models: Ridge regression, lasso, elastic net and their extensions. *BMC Proceedings*, *6*, S10. https://doi.org/10.1186/1753-6561-6-S2-S10

Paterson, A. H., Schertz, K. F., Lin, Y. R., Liu, S. C., & Chang, Y. L. (1995). The weediness of wild plants: Molecular analysis of genes influencing dispersal and persistence of Johnsongrass, *Sorghum halepense* (L.) Pers. *Proceedings of the National Academy of Sciences*, *92*, 6127–6131. https://doi.org/10.1073/pnas.92.13.6127

Piper, J. K., & Kulakow, P. A. (1994). Seed yield and biomass allocation in *Sorghum bicolor* and F_1 and backcross generations of *S. bicolor* × *S. halepense* hybrids. *Canada Journal of Botany*, *72*, 468–474. https://doi.org/10.1139/b94-062

Pritchard, A. J. (1965). Inheritance patterns in hybrids between *Sorghum almum* Parodi and perennial sweet Sudan grass. *Australian Journal of Agricultural Research*, *16*, 525–532. https://doi.org/10.1071/AR9650525

Rasmussen, J., Ntakos, G., Nielsen, J., Svensgaard, J., Poulsen, R. N., & Christensen, S. (2016). Are vegetation indices derived from consumer-grade cameras mounted on UAVs sufficiently reliable for assessing experimental plots? *European Journal of Agronomy*, *74*, 75–92. https://doi.org/10.1016/j.eja.2015.11.026

Richardson, A. J., & Wiegand, C. L. (1977). Distinguishing vegetation from soil background information. *Photogrammetric Engineering and Remote Sensing*, *43*, 1541–1552.

Rooney, W. L., Miller, F. R., & Rooney, L. W. (2003). Registration of RTx437 sorghum parental line. *Crop science*, *43*, 445–447. https://doi.org/10.2135/cropsci2003.4450

Saeed, M., Francis, C. A., & Clegg, M. D. (1986). Yield component analysis in grain sorghum. *Crop science*, *26*, 346–351. https://doi.org/10.2135/cropsci1986.0011183X002600020028x

Scheinost, P. L., Lammer, D. L., Cai, X., Murray, T. D., & Jones, S. S. (2001). Perennial wheat: The development of a sustainable cropping system for the US Pacific Northwest. *American Journal of Alternative Agriculture*, *16*, 147–151. https://doi.org/10.1017/S0889189300009115

Schnell, R., Horn, K., Biar, E., Hall, A., & Murray, S. C. (2019). *2019 Texas corn performance variety trials*. Department of Soil and Crop Sciences, Texas A&M AgriLife Research and AgriLife Extension Service. https://varietytesting.tamu.edu/files/corn/2019/2019Corn-varietytrial-results.pdf

Singh, D., Wang, X., Kumar, U., Gao, L., Noor, M., Imtiaz, M., & Poland, J. (2019). High-throughput phenotyping enabled genetic dissection of crop lodging in wheat. *Frontiers in Plant Science*, *10*, 394. https://doi.org/10.3389/fpls.2019.00394

Singh, R. K., Pratap, S. S., & Singh, S. B. (2005). Correlation and path analysis in sugarcane ratoon. *Sugar Tech*, *7*, 176–178. https://doi.org/10.1007/BF02950610

Singh, R. K., & Singh, S. B. (2002). Stability in ratooning ability of early-maturing sugarcane varieties for higher yield and recovery. *Indian Journal of Agricultural Science*, *72*, 716–718.

Stanton, C., Starek, M. J., Elliott, N., Brewer, M., Maeda, M. M., & Chu, T. (2017). Unmanned aircraft system-derived crop height and normalized difference vegetation index metrics for sorghum yield and aphid stress assessment. *Journal of Applied Remote Sensing*, *11*, 026035. https://doi.org/10.1117/1.JRS.11.026035

Sundara, B. (1997). Multiratooning potential of sugarcane varieties and management of multiratoons. *Indian Journal of Sugarcane Technology*, *12*, 24–26.

Svensgaard, J., Jensen, S. M., Christensen, S., & Rasmussen, J. (2021). The importance of spectral correction of UAV-based phenotyping with RGB cameras. *Field Crops Research*, *269*, 108–177. https://doi.org/10.1016/j.fcr.2021.108177

Vina, A., Gitelson, A. A., Rundquist, D. C., Keydan, G., Leavitt, B., & Schepers, J. (2004). Monitoring maize (*Zea mays* L.) phenology with remote sensing. *Agronomy Journal*, *96*, 1139–1147. https://doi.org/10.2134/agronj2004.1139

Washburn, J. D., Murray, S. C., Burson, B. L., Klein, R. R., & Jessup, R. W. (2013). Targeted mapping of quantitative trait locus regions for rhizomatousness in chromosome SBI-01 and analysis of overwintering in a *Sorghum bicolor* × *S. propinquum* population. *Molecular Breeding*, *31*, 153–162. https://doi.org/10.1007/s11032-012-9778-8

Watanabe, K., Guo, W., Arai, K., Takanashi, H., Kajiya-Kanegae, H., Kobayashi, M., Yano, K., Tokunaga, T., Fujiwara, T., Tsutsumi, N., & Iwata, H. (2017). High-throughput phenotyping of sorghum plant height using an unmanned aerial vehicle and its application to genomic prediction modeling. *Frontiers in Plant Science*, *8*, 421. https://doi.org/10.3389/fpls.2017.00421

Woebbecke, D. M., Meyer, G. E., Von Bargen, K., & Mortensen, D. A. (1995). Color indices for weed identification under various soil, residue, and lighting conditions. *Transactions of the ASAE*, *38*, 259–269. https://doi.org/10.13031/2013.27838

Yue, J., Yang, G., Li, C., Li, Z., Wang, Y., Feng, H., & Xu, B. (2017). Estimation of winter wheat above-ground biomass using unmanned aerial vehicle-based snapshot hyperspectral sensor and crop height improved models. *Remote Sensing*, *9*, 708. https://doi.org/10.3390/rs9070708

Zarco-Tejada, P. J., Berjón, A., López-Lozano, R., Miller, J. R., Martín, P., Cachorro, V., & De Frutos, A. (2005). Assessing vineyard condition with hyperspectral indices: Leaf and canopy reflectance simulation in a row-structured discontinuous canopy. *Remote Sensing of Environment*, *99*, 271–287. https://doi.org/10.1016/j.rse.2005.09.002

How to cite this article: Nakasagga, S., Adak, A., Murray, S. C., Rooney, W. L., Hoffmann, L., Wilde, S., Lindsey, R., Nabukalu, P., & Cox, S. (2022). Prediction of regrowth and biomass of perennial sorghum using unoccupied aerial systems. *Crop Science*, *62,* 2107–2121. https://doi.org/10.1002/csc2.20758